Journal of Thermal Analysis, Vol. 50 (1997) 19-31

Dedicated to Prof. Menachem Steinberg on the occasion of his 65th birthday

THE TEMPERATURE DEPENDENCE OF SPACE CHARGE ACCUMULATION IN CROSS-LINKED POLYETHYLENE

K. R. Bambery and R. J. Fleming

Department of Physics, Monash University, Clayton, Victoria 3168, Australia

Abstract

This paper presents the results of laser-induced-pressure-pulse (LIPP) measurements of space charge accumulation in 0.5 mm thick planar XLPE samples with aluminium electrodes, over the temperature range 30–90°C. The applied field strength was 10 kV mm^{-1}. The increase in transit time of the pressure pulse across the sample with increasing temperature indicated that Young's modulus decreased by 50% from 30 to 90°C. It was concluded that electrons injected at the cathode are transported to the anode at temperatures above 40°C, and that electron traps cause an accumulation of negative charge immediately adjacent to both cathode and anode. It appears that a concentration of impurity molecules accumulates close to the cathode, and field-assisted thermal ionisation of these molecules generates an immobile positive space charge adjoining the electronic space charge adjacent to the cathode.

Keywords: LIPP, polyethylene, space charge

Introduction

The accumulation of space charge in the insulation of electrical power distribution cables, during service lifetime, is a major cause of premature cable failure. High electric field stress tests have shown that space charge can increase the electric field strength at the insulator/conductor interface sufficiently to lower the impulse breakdown field strength of the insulator [1–5]. Furthermore, high densities of charge, either trapped or in transit, may lead to an increased rate of electrical tree formation, resulting in cable damage and eventually electrical breakdown.

Medium voltage XLPE underground power cables are usually designed to operate at temperatures up to 90°C. Increased conduction currents, indicative of increased charge mobility in the bulk and/or increased injection levels, are observed at elevated temperatures in thin films of low density polyethylene (LDPE) and cross-linked polyethylene (XLPE), two materials widely used as in-

0368–4466/97/ $ 5.00

John Wiley & Sons Limited
Chichester

sulation in power cables. Thermally stimulated luminescence and thermally stimulated current (TSC) measurements have been used to characterise the temperature dependence of the charge trapping and transport mechanisms in these materials [6–8]. Unfortunately, these techniques give an "average" view over the total thickness of the sample, rather than spatially resolved data, making detailed interpretation very difficult.

The laser-induced-pressure-pulse (LIPP) and pulsed-electro-acoustic (PEA) methods are now firmly established as reliable techniques for mapping the spatial distribution of space charge in dielectric materials, yielding both density and polarity [9–12]. Each technique reveals, within its spatial resolution limits, net space charge, but cannot distinguish between singly and doubly charged species, or between electronic and ionic charge, or between isolated charge and charge due to inhomogeneous polarisation within the sample bulk. Although much work has been done on LDPE and XLPE samples using these techniques around room temperature [13–16], there is relatively little data in the literature relating to higher temperatures [17–19]. In [19] the authors reported, perhaps rather surprisingly, that charge injection into the XLPE insulant of cylindrical cable samples under fields around 13 kV mm^{-1} was suppressed following heat treatment at 80°C for 10 days under rotary pump pressure. Other authors of [17] found that charge injected into planar LDPE samples at temperatures above 50°C and 40 kV mm^{-1} was immediately discharged to the electrodes when the samples were shorted. Both sets of authors employed the PEA technique. There appears to be only one paper in the literature [18] presenting LIPP data on the effect of temperature on space charge accumulation; although two different kinds of LDPE cable insulant were studied, the experiments were conducted only at 50°C.

In this paper we present LIPP data for planar XLPE samples cut from the insulation of 22 kV power cables, and subjected to DC fields of strengths up to 10 kV mm^{-1} at temperatures in the range 30–90°C.

Experimental

Samples in the form of sheets measuring 5 cm×5 cm×0.5 mm were peeled from lengths of commercial power cable, using a wide cutting blade on a metal turning lathe. The cables had been manufactured using dicumyl peroxide (DCP) cross-linking and dry nitrogen curing in the continuous catenary vulcanisation (CCV) method [20]. Aluminium electrodes 1.5 or 3 mm thick were attached to both surfaces of each sample using a very thin layer of a silver-doped epoxy adhesive (Allied Products Corp. E-Solder No. 3021). Aluminium is a suitable laser target electrode because of its low acoustic dispersion and attenuation properties [21].

The LIPP experimental arrangement used for the space charge measurements is illustrated in Fig. 1. A 5 ns laser pulse with wavelength 1064 nm impinges on

the target (ground) electrode, thereby generating an ultrasonic pressure pulse which propagates across the sample. The pulse compresses the sample material, changing its relative permittivity, and also causes a transient displacement of the space charge. The current thereby induced on the non-grounded electrode at time t can be related to the space charge density at position x, where $x=ct$ and c is the speed of longitudinal sound waves in the sample [9, 10].

The target electrode can be heated and its temperature measured by an adjacent thermocouple. Temperature control is achieved using a Eurotherm 815 con-

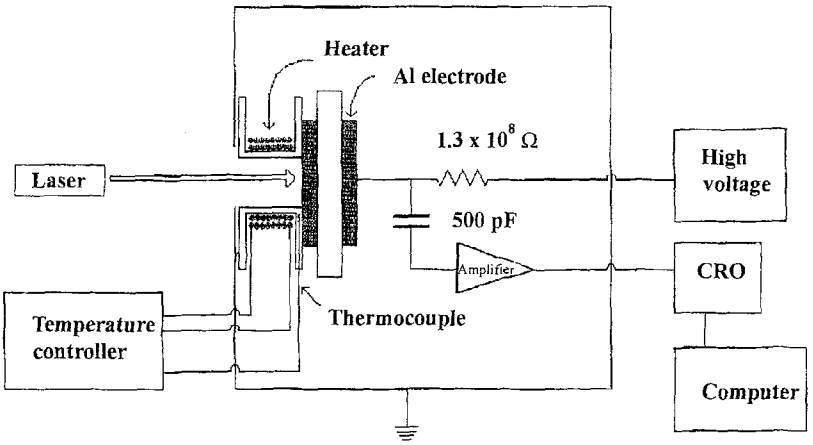

Fig. 1 LIPP experimental setup for the measurement of charge distribution

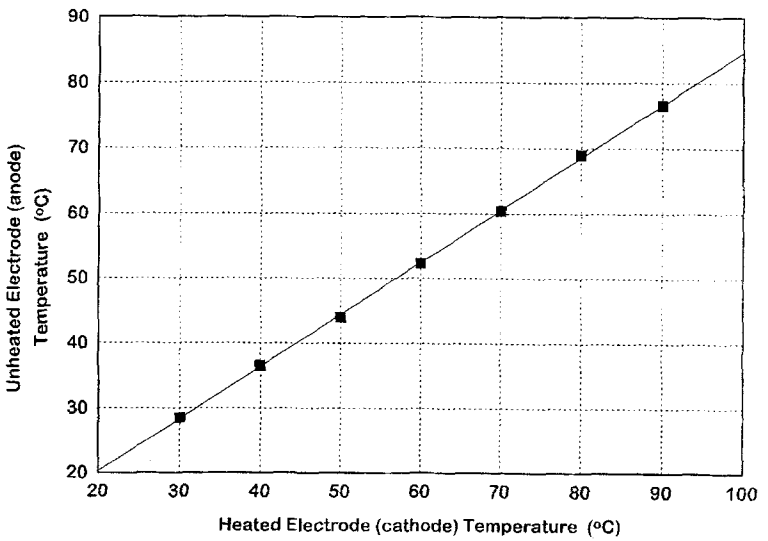

Fig. 2 Unheated electrode temperature as a function of the heated electrode temperature (in thermal equilibrium)

troller connected to the heater. The samples are heated only on the ground side because of the practical difficulties of attaching a heater to the HT electrode. Consequently a temperature gradient exists across the thickness of the samples during measurement. The magnitude of this gradient was estimated by attaching an additional thermocouple to the HT electrode with no electric field applied, and recording the temperatures of both sides of the sample in thermal equilibrium (Fig. 2). In the remainder of this paper, quoted temperatures relate to the target electrode.

In all the measurements, conducted in laboratory air, the laser-irradiated target electrode was the cathode (ground potential) and the HT electrode was the anode. The input impedance of the amplifier was 50 Ω, so that the oscilloscope traces yielded directly the space charge density in the bulk of the sample [22]. Since the sample materials were all "extra-clean" inclusion-free quality, we assume that negligible polarisation gradients existed. The gain of the amplifier was 26 dB over the frequency range 100 kHz–1.4 GHz. Except for the calibration measurements, the applied field strength was 10 kV mm^{-1}.

Results and discussion

Space charge density calibration

The samples were heated from 30 to 90°C in 10°C increments. At each increment, after the anode temperature had stabilised, a weak electric field (1.0 kV mm^{-1}) was applied and a LIPP trace obtained. The field was then turned off. We assume that, with a low field applied for only about 3 min, no space charge accumulates in the sample bulk. The trace then shows only the charges on the anode and cathode due to the applied voltage. When this procedure was repeated at 0.5 and 1.5 kV mm^{-1} for some samples, a linear relationship between signal amplitude and field strength was observed. These data were used to calibrate space charge density accumulating in the sample bulk when larger field strengths were applied. Specifically,

$$\rho(x) = \frac{V(t)}{V_{cal}} \frac{\varepsilon_o \varepsilon_r}{c\tau} E_{cal} \tag{1}$$

where $\rho(x)$ is the net space charge density at position x, $V(t)$ is the amplitude of the signal at time t, ε_o and ε_r have their usual meanings, c is the speed of longitudinal sound waves in XLPE, τ is the duration of the pressure pulse (taken nominally as the width of the cathode signal at half maximum height), V_{cal} is the magnitude of the cathode signal observed under a low applied field E_{cal}, and $x=ct$. No attempt was made to correct the traces for attenuation or dispersion of the pressure pulse in transit through the sample.

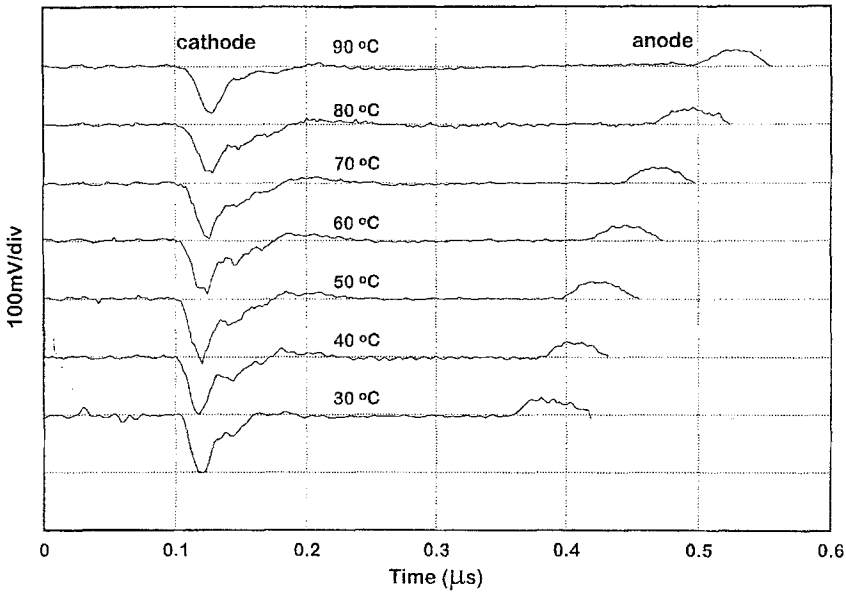

Fig. 3 Calibration traces at various temperatures for an applied field of 1 kV mm
The dotted horizontal line running through each trace is the zero for that trace

Figure 3 shows typical calibration traces at six different temperatures. The negative peak centred around 0.12 μs is due to the voltage-induced charge on the surface of the cathode. The positive peak due to the charge on the anode occurs between approximately 0.41 and 0.53 μs. A small negative peak, due to reflection of the pressure pulse from the XLPE/anode interface and re-entry into the XLPE, appeared shortly after the anode signal, and has been suppressed in the traces presented below. In the absence of bulk space charge, the charges on the anode and cathode surfaces are equal and opposite. However, the anode signal is weaker and broader than the cathode signal because of attenuation and dispersion of the pressure pulse in transit between the electrodes. From Fig. 3 it is evident that the transit time of the pressure pulse from cathode to anode increases with increasing temperature. At 30°C the speed of sound calculated from the transit time is 1.8 km s^{-1}, which agrees well with the expected value 1.95 km s^{-1} [23]. We have

$$t_{tr}(T) = \frac{d(T)}{v(T)} \tag{2}$$

where $t_{tr}(T)$, $d(T)$ and $v(T)$ are the transit time, sample thickness and speed of sound respectively at temperature T. The transit time was taken as the time between the peaks of the anode and cathode signals. Since

$$d(T) = d_o(1+\alpha\Delta T) \tag{3}$$

and

$$v(T) = \sqrt{\frac{E(T)}{\rho(T)}} \tag{4}$$

where α, E and ρ are respectively the linear coefficient of expansion, Young's modulus and density, $\Delta T=T-T_o$ and d_o is the thickness of the sample at T_o, it follows that, assuming isotropic thermal expansion of the sample,

$$t_{tr}(T) = d_o\sqrt{\frac{\rho_o}{E(T)(1+\alpha\Delta T)}} \tag{5}$$

where ρ_o is the sample density at T_o. Taking ρ_o as 920 kg m^{-3} at 20°C and α as 2.25×10^{-4} °C^{-1} [24], we find that Young's modulus for the samples decreases from about 3×10^9 Pa at 30°C to 1.5×10^9 Pa at 90°C. These values are certainly of the expected order of magnitude [25].

In order to facilitate comparison of the space charge distribution at different temperatures, the horizontal axes of the traces presented below have been calibrated in terms of distance through the sample. On the calibration traces the peak of the cathode signal was taken as the time at which the pressure wave peak passed through the cathode/XLPE interface, and the interval between it and the laser firing time noted. On the higher field traces t=0 coincides with the end of this same interval. Distance through the sample was then calculated by multiplying time by the speed of sound at the appropriate temperature. Using this procedure, t=0 always coincides with the peak of the cathode signal in field-applied measurements, because the voltage-induced charge on the cathode surface dominates the bulk space charge. However, in short-circuit there is no voltage-induced charge, and the space charge immediately adjacent to the cathode induces an opposite and nearly equal charge on the cathode surface. The finite width of the pressure pulse then causes the induced charge to appear as if it were located behind the cathode. In Figs 4–9 the cathode and anode positions are indicated by thick vertical lines.

Charge accumulation with time under an applied field

The field was applied to each sample at 40°C for 5 min. The sample was then short-circuited and the trace obtained as quickly as possible (within less than 2 min). The field was re-applied for 10 min, the sample short-circuited and another trace recorded. This procedure was continued, increasing the time of field application at each cycle, until no further changes in the trace were observed.

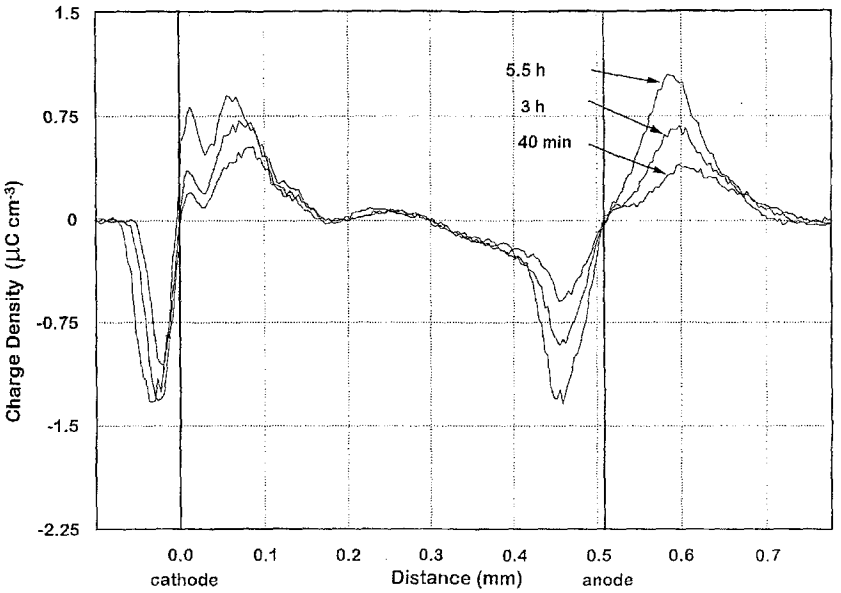

Fig. 4 Evolution of space charge under the influence of a 10 kV mm^{-1} applied field at 40°C. The traces were recorded in short-circuit

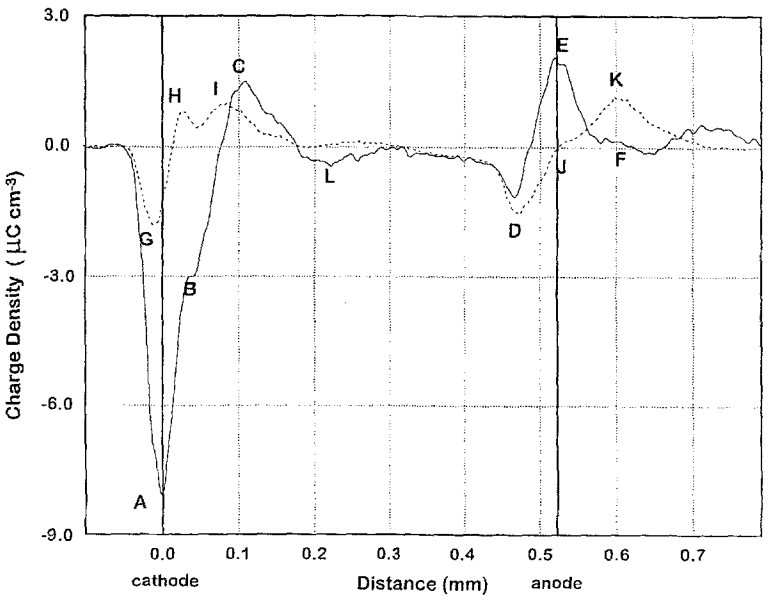

Fig. 5 Field-applied trace (solid line) and short-circuit trace (dashed line) after 5.5 h at 10 kV mm^{-1} and 40°C

This equilibrium was reached after about 5.5 h total field application time. Figure 4 shows the short-circuit traces obtained after the field had been applied for 40 min, 3 and 5.5 h. There was no obvious reduction in signal intensity if the sample was allowed to sit in short-circuit for several minutes (at 40°C).

Figure 5 shows the field-applied and short-circuit traces (solid and dashed lines respectively) obtained after the field had been applied for 5.5 h. As stated above, in short-circuit the charge on the electrodes is that induced by the bulk space charge; with the field applied, there is an additional component due to the applied voltage. On the field applied trace, points A and E are the signal peaks due to the total charge on the cathode and anode respectively, B is thought to be an instrumental artefact, C indicates the presence of considerable positive space charge in the bulk adjacent to the cathode, L is due to electrons in transit from cathode to anode, and D is due to negative space charge in the bulk adjacent to the anode. The small plateau at F is generated when the pressure pulse, considerably broadened in transit across the sample, is reflected from the XLPE/aluminium interface, and interacts simultaneously with the positive charge on the anode and the trapped negative space charge immediately adjacent to it. The reflection coefficient for this interface, defined as $(Z_{Al}-Z_{XLPE})/(Z_{Al}+Z_{XLPE})$, where Z=acoustic impedance=$(\rho E)^{1/2}$ [12], is approximately 0.8. On the short circuit trace, point G is the signal peak due to the induced charge on the cathode, H and I again indicate positive space charge in the bulk adjacent to the cathode, D is again due to negative space charge in the bulk adjacent to the anode, while J and K originate in passage of the reflected pressure pulse through the induced charge on the anode and the negative space charge respectively. In relation to H, I and C, we suggest that the positive space charge originates in field-assisted ionisation of impurities, probably cross-linking residues, which had migrated towards the XLPE surface before measurements were commenced [19 and references therein]. The density of this charge increases when the field is applied, presumably because more of the impurities are ionised. The trapped negative charge at D presumably consists of electrons liberated from the ionised impurities near the cathode and others injected at the cathode. The negative peak (at D) decreases when the field is applied because the broadened pressure pulse interacts simultaneously with the trapped negative charge and the positive charge on the anode due to the applied voltage.

When the measurements were repeated at 90°C, very similar traces were obtained (Fig. 6). However, the charge distribution stabilised much more rapidly, i.e. the short-circuit trace did not vary provided the field had been applied for at least 10 min, compared with 5.5 h at 40°C.

Short-circuit isothermal discharge

In order to study the stability of the bulk space charge, the field was applied for 1 h at 40°C and the sample short-circuited. Measurements were then made

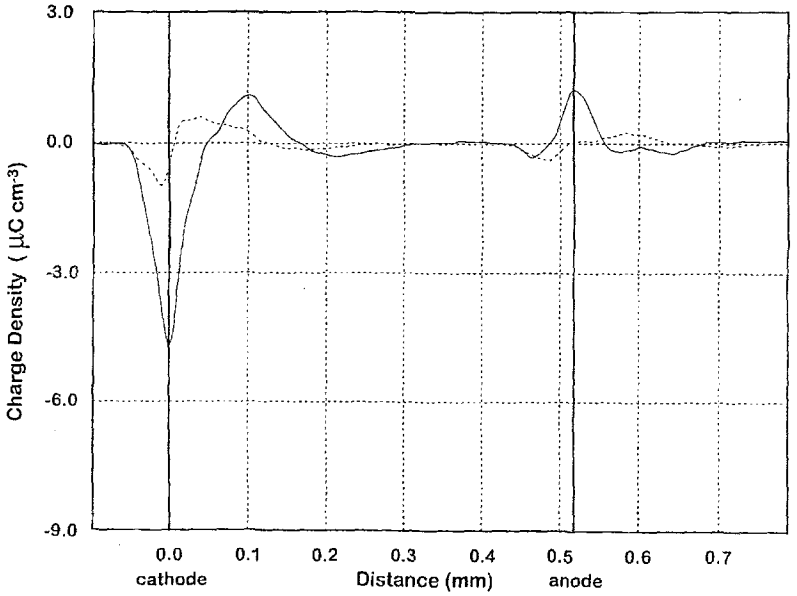

Fig. 6 Field-applied trace (solid line) and short-circuit trace (dashed line) after 5.5 h at 10 kV mm^{-1} and 90°C

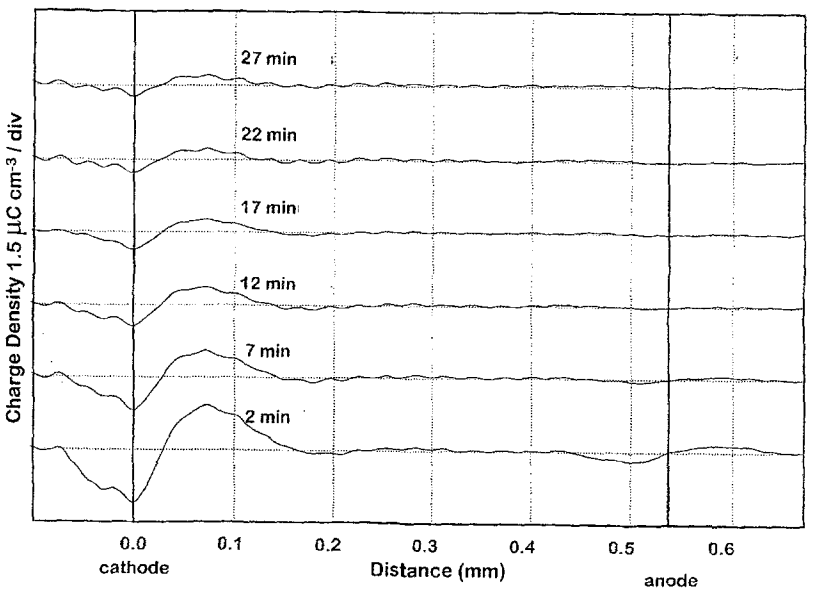

Fig. 7 Short-circuit traces obtained at 90°C, following application of *A* 10 kV mm^{-1} field for 1 h at 90°C. The dotted horizontal line running through each trace is the zero for that trace

after various times. The reduction in signal amplitude with time in short-circuit was very small, e.g. 7% loss in the first 10 min and an additional 7% over the next 7 days. On the other hand, when this procedure was repeated at 90°C the signal intensity dropped rapidly, as shown in Fig. 7. Note that no signal was detected from the anode after about 12 min. The moderate attenuation of the pressure pulse in transit across the sample at 90°C, shown in Fig. 3, suggests that the disappearance of the anode signal should be attributed to transport of the trapped electrons over the potential barrier at the anode. The disappearance of the cathode signal is attributed to electron injection from the cathode, under the combined influence of high temperature and attraction towards the ionised impurities, followed by recombination with the latter. Since the cathode signal disappears more slowly than the anode signal, we deduce that the potential barrier for electron transport is higher at the cathode than at the anode.

Field application at increasing temperatures

The field was applied for 1 h at 30°C. The sample was then short-circuited and a measurement made as quickly as possible. After heating to 40°C with the field applied, the sample was held at that temperature for 1 h and short-circuited. A second measurement was then made and the procedure repeated in 10°C increments up to 90°C. The results are presented in Fig. 8. The signal at the anode increases in amplitude from 30 to 50°C, then decreases steadily up to 90°C. At

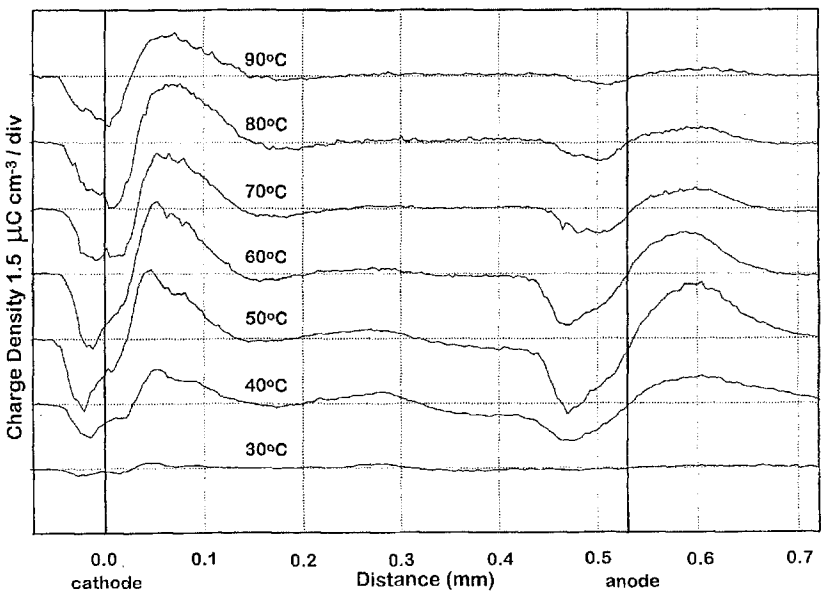

Fig. 8 Short-circuit traces after a 10 kV mm^{-1} field had been applied at the indicated temperatures for 1 h. The dotted horizontal line running through each trace is the zero for that trace

the cathode the signal again increases from 30 to 50°C but is then nearly constant. The initial increase in negative space charge adjacent to the anode is attributed to accumulation of electrons transported across the sample from the cathode (injected and generated by ionisation of impurities). It appears that, above 50°C, increasing thermal excitation over the barrier more than compensates for an expected increase in charge transport from the cathode. We suggest that the nearly constant positive space charge density adjacent to the cathode above 50°C results from complete ionisation of the available impurity molecules, and a low probability of recombination with electrons when the field is applied. A charge density of 1.2 μC cm^{-3} (above 50°C) corresponds to 7.5×10^{12} ionised molecules cm^{-3}. The accumulation of trapped negative space charge immediately adjacent to the cathode indicates that charge is being injected faster than it can be transported to the anode. Electron traps are expected to exist throughout the volume of the sample, perhaps in increased concentration at the surfaces.

Thermal step discharging

The field was applied at 90°C for 1 h, after which the sample was cooled to 30°C with the field still applied and maintained at that temperature for 1 h (to allow thermal equilibrium to be established). It was then short-circuited and a

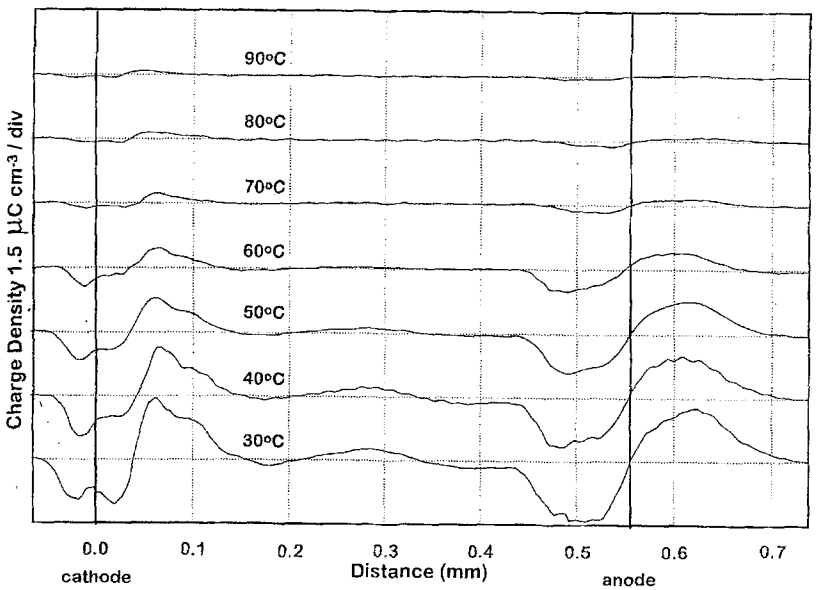

Fig. 9 The sample was maintained at 90°C for 1 h under a 10 kV mm^{-1} field, and then cooled to 30°C with the field still applied. The short-circuit traces were then recorded in 10°C steps from 30–90°C. The sample stood at each temperature for 10 min before the measurement was made. The dotted horizontal line running through each trace is the zero for that trace

measurement made. Further measurements were made at 10°C intervals up to 90°C, the sample having stood at each temperature for 10 min before the measurement was made.

The results are presented in Fig. 9. The principal feature is the gradual disappearance of the signal from both electrodes with increasing temperature. At 30°C a large concentration of trapped electrons exists adjacent to the anode, these electrons having transited across the sample from the cathode and fallen into traps of varying depths as the temperature was lowered from 90 to 30°C. When the sample was heated, they escaped from the traps and were extracted at the anode. Consequently the positive charge induced on the anode disappeared.

At 30°C there exists immediately adjacent to the cathode a concentration of trapped electrons injected from the cathode, with impurity positive ions more distant from the cathode (0.04 to 0.14 mm). When the temperature is raised the electrons escape from the shallower traps and recombine with the positive ions. However, since the positive ion charge at 30°C considerably exceeds the trapped electron charge, the nearly complete neutralisation of the positive charge at 90°C implies electron injection from the cathode. The reduction in both positive and negative charge between 30 and 40°C might at first sight appear inconsistent with the stability of the trace when the field was applied at 40°C and the sample short circuited, as mentioned above. However, Fig. 9 relates to the situation where the field was applied continuously while the sample cooled from 90 to 30°C. This procedure results in a concentration of trapped electrons at 30°C larger than that resulting from application of the field at 30°C only. The resulting change in the local electric field could well reduce the effective trap depths.

Conclusions

The following conclusions may be drawn from this work:

1) Above 40°C and at an applied field strength of 10 kV mm^{-1}, transport of injected electrons across the sample from cathode to anode occurs.

2) Electron traps in the sample bulk immediately adjacent to the anode and the cathode, along with charge injection from the cathode and a potential barrier at the anode, lead to a build-up of negative space charge adjacent to both electrodes.

3) Very little charge accumulates in the bulk well away from the electrodes, probably because the trap concentration is lower in the bulk than near the surfaces.

4) Very few of the electron traps retain electrons at temperatures above approximately 80°C.

5) It appears that a concentration of impurity molecules develops close to the cathode. Field assisted ionisation of these impurities, and transport of the associated electrons to the anode, leads to a build-up of positive space charge close

to the cathode, adjoining the negative space charge. A similar concentration of impurities would be expected close to the anode, but the accumulation of negative space charge in that region prevents the impurities being permanently ionised.

* * *

The authors wish to thank MM Cables, Sydney for providing lengths of XLPE power cable from which the samples were cut. K.R.B. acknowledges the award of an Australian Postgraduate Research Award (Industry), and R.J.F. thanks the Australian Research Council for financial support to purchase the laser used in the measurements.

References

1 A. Bradwell, R. Cooper and B. Varlow, Proc. IEE, 118 (1971) 247.
2 M. Ieda, IEEE Trans. Electr. Insul., 22 (1977) 261.
3 T. Mizutani, IEEE Trans. Dielect. Electr. Insul., 1 (1994) 923.
4 M. Mammeri and C. Laurent, IEEE Trans. Dielect. Electr. Insul., 2 (1995) 27.
5 M. Ieda, M. Nagao and M. Hikita, IEEE Trans. Dielect. Electr. Insul., 1 (1994) 934.
6 R. J. Fleming, J. Thermal Anal., 36 (1990) 331.
7 A. Markiewicz and R. J. Fleming, J. Phys. D: Appl. Phys., 21 (1988) 349.
8 K. Doughty, D. K. Das-Gupta and D. E. Cooper, Annual Report, CEIDP (IEEE), New Jersey 1986, p. 56.
9 C. Alquié, G. Dreyfus and J. Lewiner, Phys. Rev. Lett., 47 (1981) 1483.
10 G. M. Sessler, J. E. West, and G. Gerhard, Phys. Rev. Lett., 48 (1982) 563.
11 T. Maeno, T. Futami, H. Kusibe, T. Takada and C. M. Cooke, IEEE Trans. Electr. Insul., 23 (1988) 433
12 J. B. Bernstein, IEEE Trans. Electr. Insul., 27 (1992) 152.
13 T. Ditchi, C. Alquie, J. Lewiner, E. Favrie and R. Jocteur, IEEE Trans. Electr. Insul., 24 (1989) 403.
14 G. A. Cartwright, A. E. Davies, S. G. Swingler and A. S. Vaughan, IEE Conf. Publ., 363 (1992) 119.
15 Y. Li and T. Takada, J. Phys. D: Appl. Phys., 25 (1992) 704.
16 N. Hozumi, H. Suzuki, T. Okamoto, K. Watanabe and A. Watanabe, IEEE Trans. Diel. Electr. Insul., 1 (1994) 1068.
17 Seung Hwang-Bo, Jin-Kyun Kim, Dong-Yung Yi and Min-Koo Han, Proc. 5th Int. Conf. on Conduction and Breakdown in Solid Dielectrics (ICSD), IEEE, Leicester (1995) p. 169.
18 S. Mahdavi, C. Alquie and J. Lewiner, Jicable 91 Section B8, 534.
19 X. Wang, D. Tu, Y. Tanaka, T. Muronaka, T. Takada, C. Shinoda and T. Hashizumi, IEEE Trans. Diel. Electr. Insul., 2 (1995) 467.
20 D. McAllister and D. Pollard, in Electric Cables Handbook 2nd Ed., Ed. E. W. G. Bungay and D. McAllister, CRC Press, Boca Raton 1990.
21 C. Alquie, J. Lewiner and G. Dreyfus, J. Phys. Lett., 44 (1983) L-171.
22 R. J. Fleming, M. Molby Henriksen, M. Henriksen and J. T. Holbrall, Proc. 5th Int. Conf. on Conduction and Breakdown in Solid Dielectrics (ICSD), IEEE, Leicester 1995 p. 234.
23 CRC Handbook of Chemistry and Physics, CRC Press, Boca Raton, 73rd Ed. 1992–93, p. 14–31.
24 ICI Cablecom Wire and Cable Compounds – Union Carbide HFDE–4201 EC Power Cable Insulation (1990).
25 S. Matsuoka, Relaxation Phenomena in Polymers (Hanser, New York) 1992, Ch. 5.